Synthesis and characterization of LNMO cathode materials for lithium-ion batteries

Available online at www.sciencedirect.com

ScienceDirect

Materials Today: Proceedings 5 (2018) 27416–27424

materialstoday: PROCEEDINGS

www.materialstoday.com/proceedings

PSCCE_2017

Synthesis and characterization of LNMO cathode materials for lithium-ion batteries

Ganas, G.[a]*, Kastrinaki, G.[a], Zarvalis, D.[a], Karagiannakis, G.[a], Konstandopoulos, A.G.[a,b], Versaci, D.[c], Bodoardo, S.[c]

[a]*Aerosol & Particle Technology Lab., Chemical Process & Energy Resources Inst., Centre for Research & Technology Hellas (APTL/CPERI/CERTH), 6th km Charilaou-Thermi, 57001, P.O. Box: 361, Thermi-Thessaloniki, Greece*

[b]*Dept. Chemical Engineering, Aristotle Univ. of Thessaloniki (AUTH), Thessaloniki, 54124, Greece*

[c]*Department of Applied Science and Technology, Politecnico di Torino, Corso Duca degli Abruzzi 24, 10129 Torino, Italy*

Abstract

Synthesis of $LiNi_{0.5}Mn_{1.5}O_4$ (LNMO), a promising cathode material for next generation lithium-ion batteries, was performed via Liquid Phase Self-propagating High-temperature Synthesis (LPSHS) and Aerosol Spray Pyrolysis (ASP) techniques. In the case of the LPSHS technique, the effect of the "fuel" quantity of the precursor solution on the structure, morphology and electrochemical performance of the materials was studied, while in the case of the ASP technique the effect of eight different calcination profiles on the structure, morphology, crystalline phase and electrochemical performance of the material. Structural characterization was performed through XRD, SEM, TEM, BET and Raman spectroscopy, while the electrochemical activity was evaluated via charge/discharge galvanostatic characterization. The results showed that the optimal LPSHS material was obtained for a molar ratio of metal ions/fuel = 3:1 exhibiting stable specific capacity over the cycles even by increasing the C-rate. The optimal ASP material was identified in the case of calcination at 850°C. Both materials had the disordered *Fd*-3*m* structure of the LNMO spinel.

Selection and/or Peer-review under responsibility of 11th Panhellenic Scientific Conference on Chemical Engineering.

Keywords: High-voltage cathode material; LNMO; Spinel; Li-ion battery; Aerosol Spray Pyrolysis

* Corresponding author. Tel.: +30-231-049-8291; fax: +30-231-049-8190.

E-mail address: ganas@cperi.certh.gr

Selection and/or Peer-review under responsibility of 11th Panhellenic Scientific Conference on Chemical Engineering.

1. Introduction

The ever-increasing environmental issues along with the inevitable depletion of fossil fuels have given great concern to the development and utilisation of renewable energies. The development of next-generation Lithium-ion battery technology with improved lifespan, energy and power density is one of the most important challenges for the implementation and wider commercialization of electric vehicles [1]. To achieve this goal, a solution would be the development of suitable cathode materials as well as compatible electrolytes. A large number of cathode materials has been explored extensively such as layered $LiMO_2$ [2-5] olivine $LiMPO_4$ [6-8] and spinel LiM_2O_4. One promising material of the latter category is $LiNi_{0.5}Mn_{1.5}O_4$ (LNMO) due to its high charge/discharge potential (~4.7 V vs Li/Li^+), good theoretical specific capacity (~147 mAh/g) [9], and its environmental friendliness [10, 11].

LNMO appears in two different space groups, namely the ordered single cubic $P4_332$ and the disordered face-centered *Fd*-3*m* structure. In the $P4_332$ case, Mn^{4+} and Ni^{2+} ions are located at 12d and 4a sites respectively, with the absence of Mn^{3+} ions, while Li ions are allocated at 8c sites and O at 8c and 24e sites. In the *Fd*-3*m* case, Mn^{4+} and Ni^{2+} ions are randomly distributed at 16c sites of the lattice, while Li and O are located at 8a and 32e sites respectively [12]. Unlike the $P4_332$ structure which exhibits a stoichiometric amount of oxygen atoms, the disordered *Fd*-3*m* demonstrates oxygen vacancies, δ, thus leading to $LiNi_{0.5}Mn_{1.5}O_{4-\delta}$ structure with certain Mn ions being reduced to Mn^{3+} for charge balancing reasons [13].

The factor determining whether the material follows the ordered $P4_332$ or disordered *Fd*-3*m* space group is the heat treatment conditions. In particular, the disordered *Fd*-3*m* space group can be attained through calcination at temperatures >700°C (e.g. 800-1000°C) [14-16] while the ordered $P4_332$ is obtainable through two possible ways: a) a two-step calcination process with the first step being carried out at high temperatures (800-1000°C) and the second step at 700°C in air atmosphere [17, 18] and b) through a two-step calcination with the second step performed at ≤700°C in O_2 atmosphere [19, 20]. The determination of the two groups is possible through Raman spectroscopy. According to Amdouni et al. [21], more peaks are expected to appear in the $P4_332$ case than in *Fd*-3*m*. In particular, in both space groups a high-intensity peak appears at a wavenumber of ~636 cm^{-1} which is attributed to the symmetrical vibration of Mn-O bond of MnO_6 octahedra. In addition, an extra peak is expected at ~490 cm^{-1}, which corresponds to the Ni^{2+}-O lattice bond vibration. In the $P4_332$ space group, an extra peak at ~400 cm^{-1} appears (Ni^{2+}-O bonds) as well as additional peaks at 220 cm^{-1}, 240 cm^{-1} and a double of peaks at 590 cm^{-1} suggesting a good dispersion of the Ni and Mn positions due to the reduced symmetry of the $P4_332$ structure [22].

Despite its advantages, LNMO may exhibit significant reduction in capacity during cycling. This may occur due to Mn diffusion in the mass of the electrolyte mass caused from various lattice modifications accompanied by the Jahn-Teller effect [23]. Studies have shown that the LNMO synthesis method does not only affect morphology, particle size and crystallinity, but also plays a key role in stoichiometry, crystal structure, impurities, and thus the electrochemical performance [24]. Numerous synthesis methods such as solid-state [25-27], co-precipitation [28-29], sol-gel [30], molten salt [31-33], emulsion drying [34, 35] and hydrothermal route [36] have been pursued in order to improve the electrochemical performance of LNMO. Good review papers (ref. [37-42]), demonstrate the electrochemical performance of differently synthesized LNMO materials. However, the presented results are not easily comparable since performance, at the cell level, depends on many parameters (electrolyte, electrode formulation, cell design, charging/discharging method, etc.) which vary among the different research groups.

In this work, two techniques, suitable for synthesising mixed oxide systems, are employed for the LNMO synthesis. The first is Liquid Phase High-temperature Self-propagating Synthesis (LPSHS), which is based on a modification of the Pechini method [43], is a one-step bulk synthesis process and has been extensively used for the rapid synthesis of both simple and mixed oxides with controllable stoichiometry and morphology [44-46]. The second technique is Aerosol Spray Pyrolysis (ASP), a one-step cost-effective technique that provides good control of the process parameters and thus, good control of particle size, stoichiometry and morphology of the resulted materials [47]. ASP also has been widely used for the synthesis of nanostructured mixed oxides [48-50].

2. Experimental

2.1. Material synthesis

2.1.1. LPSHS

In LPSHS method, a precursor solution of 1M on the basis of total metal ions was prepared by dissolving stoichiometric amounts of the desired Li, Ni and Mn metal precursors in distilled water ("oxidant") along with a certain amount of an organic compound ("fuel"). The resulted solution was heated at 80^{o}C under continuous stirring, resulting in gel formation. By further increasing the temperature, the gel was self-ignited, ultimately forming a precursor material in powder form. After calcination at 850°C, the final LNMO powders were obtained [44]. Three different LNMO materials were synthesised using different metal ions/fuel molar ratio in the precursor solution (Table 1).

Table 1. Summary of LNMO samples synthesised via LPSHS.

Sample	Metal ions/fuel molar ratio	Calcination profile (air atmosphere)
LP-1	1:1	
LP-2	2:1	850°C
LP-3	3:1	

2.1.2. ASP

Concerning the ASP technique, similarly, a precursor solution of 1M on the basis of total metal ions was prepared by dissolving stoichiometric amounts of Li, Ni and Mn precursors in distilled water. According to the ASP principle, the precursor solution is sprayed, and, with the aid of a carrier gas (in this study air was used) the resulting droplets are transferred to the interior of a heated tubular reactor. When the droplets move through the hot zone of the reactor, evaporation of the solvent takes place, thus resulting in the formation of solid particles in powder form. After calcination, the final LNMO powder is formed [47]. In the present study, eight different LNMO materials were produced using different calcination profiles (Table 2).

Table 2. Summary of LNMO samples synthesised via ASP.

Sample	Precursor Solution Molarity (*M*)	Synthesis Temperature (°*C*)	Calcination Profile
ASP-1	1.0	800	700°C, air
ASP-2			800°C, air
ASP-3			850°C, air
ASP-4			900°C, air
ASP-5			800°C → 700°C, air
ASP-6			850°C → 700°C, air
ASP-7			900°C → 700°C, air
ASP-8			700°C → 900°C → 700°C, air

2.2. Characterization

The phase structure of the materials was identified by XRD analysis using a Siemens D500/501 X-ray diffractometer with Cu Kα radiation between 5° and 80° at a scan rate of 0.040 °/s. The morphology of the prepared samples was observed by a scanning electron microscope (JEOL JSM-6300) and a high-resolution transmission electron microscope (JEOL JEM 2010). The LNMO space groups were identified with a micro-Raman Spectrometer

(Renishaw inVia Reflex). The specific surface area of the samples (BET method) was measured through a N_2 adsorption porosimeter (Micromeritics ASAP 2000, at 77 K, after degassing the samples at 250°C).

2.3. Electrode preparation

A N-methyl-2-pyrrolidone (NMP, Aldrich) based slurry of the as-prepared LNMO sample was mixed with carbon black (C65 from Imerys Graphite & Carbon) as electronic conduction enhancer and poly-(vinylidenefluoride) as binder (PVdF, Kynar 761), in the weight ratio of 90:5:5. A 4% w/w PVdF solution in NMP was weighed and transferred into appropriate beaker while the solid fraction of LNMO and conductive additive carbon was separately mixed by a mortar and finally slowly added to the liquid fraction. The complete mixture was stirred for 4h.

The working electrodes were prepared by a solvent tape casting method, where the slurry was mechanically deposited on an aluminum current collector, (standard practice in Li-ion battery testing), using a Doctor Blade adjusted for 300 μm deposition and an automatic film applicator (Sheen 1133N) with a speed of 50 mm/s. After evaporating the solvent in air, disks with a surface of 0.8 cm^2 were punched out and vacuum dried at 120 °C (Büchi Glass Oven B-585) for 4 h, then transferred into an Argon filled dry glove-box (MBraum Labstar, H_2O and O_2 content < 1 ppm) where the disks were weighed and the cells assembled. The composite electrodes were placed in a Polypropylene three-electrode T-cells with lithium foil (Chemetall Foote Corporation) as counter and reference electrode and two glass-wool disks (Whatmann GF/A) as the separator. The liquid electrolyte was provided by ARKEMA and was optimised for the LNMO cathode.

3. Results

3.1. LPSHS

Fig. 1(a) depicts the XRD spectra of the resulted LNMO materials. In all three cases of metal ions/fuel molar ratio, the spectra peaks correspond to the $LiNi_{0.5}Mn_{1.5}O_4$ structure with a slight difference in sample LP-3 (molar ratio 3:1) where the additional peaks at diffraction angles 56°, 37° and 63° indicate that fuel-leaner synthesis resulted in the formation of impurities. Crystallite size (Fig. 1(b)) was calculated by Scherrer formula. The results reveal that increasing the metal ion/fuel molar ratio from 1:1 to 2:1 and 3:1 led to crystallite size decrease from 55 nm to 49 nm and 35 nm, respectively.

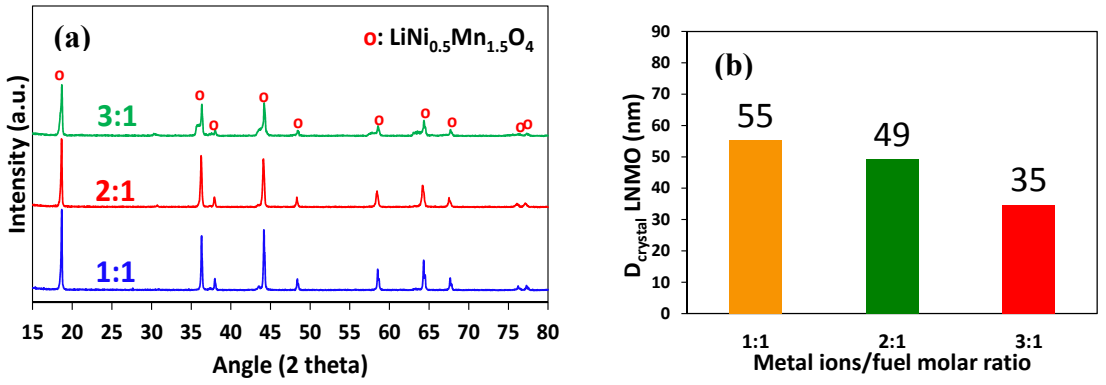

Fig. 1. (a) XRD spectra and (b) crystallite size of LNMO synthesised via LPSHS.

SEM analysis (Fig. 2) revealed that in the 1:1 molar ratio case the particles gained a polyhedral structure, while increasing to 2:1 a slight increase in the particle size was observed. In the 3:1 molar ratio case spherical formations consisting of smaller polyhedral particles were formed. BET results showed that molar ratio increase led to decrease of LNMO surface area, namely from 2.22 m^2/g to 1.74 m^2/g and 0.77 m^2/g for ratios 1:1, 2:1 and 3:1 respectively.

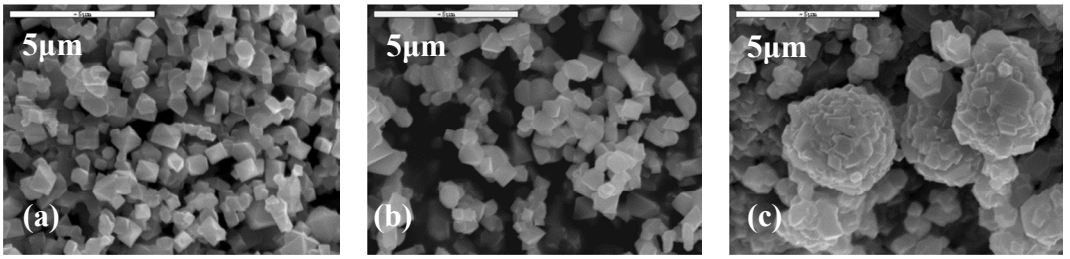

Fig. 2. SEM images of LNMO synthesised via LPSHS for metal ions/fuel molar ratios of: (a) 1:1, (b) 2:1 and (c) 3:1.

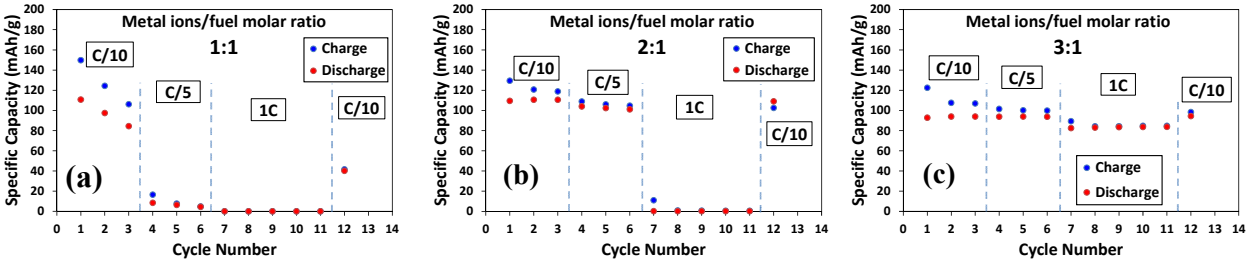

Fig. 3. Electrochemical performance of LPSHS synthesised LNMO materials for metal ions/fuel molar ratios of (a) 1:1 (b) 2:1 and (c) 3:1.

Fig. 3 demonstrates the electrochemical performance of the LNMO materials. The evaluation included three electrochemical cycles at C/10, three cycles at C/5, five cycles at 1C and one cycle at C/10. Using a 1:1 metal ions/fuel molar ratio (Fig. 3(a)), the discharge specific capacity at C/10 rate was reduced from ~110 mAh/g (1st cycle) to ~75 mAh/g (3rd cycle). By increasing C-rate at C/5, the specific capacity displayed a sharp decrease (~10 mAh/g) while for 1C rate it exhibited zero values. Increasing the molar ratio to 2:1 (Fig. 3(b)) resulted in specific capacity improvement at lower C-rates (C/10 and C/5) with a value of ~110 mAh/g and zero values at 1C. Using a 3:1 molar ratio (Fig. 3(c)) high stability at C/10 and C/5 was observed, however, with moderately decreased specific capacity (~90-95 mAh/g).At 1C rate, a further slight decrease was observed (~85 mAh/g), but with good stability over the cycles. Further commenting on the cyclic stability aspect and on the basis of the 12th charge/discharge cycle at C/10, the 2:1 and 3:1 compositions exhibited specific capacity values close to the ones noted in the initial cycles. Concerning the best performing material (3:1 metal ions/fuel molar ratio), the specific capacity is relatively close to the theoretical value of 147 mAh/g [9] at low C-rate values. Despite its good cyclic stability at higher C-rates, further improvement is need. To this respect and based on the analysis presented here, additional parametric studies regarding the metal ions/fuel molar ratio, fine tuning of calcination temperature and duration as well as measures to eliminate observed impurities are currently underway.

3.2. ASP

According to the XRD spectra (Fig. 4(a)), the desired LiNi0.5Mn1.5O4 phase was obtained for all eight calcination profiles. Raman spectroscopy results are presented in Fig. 4(c) revealing that LNMO samples ASP-1, ASP-5, ASP-6 and ASP-7 correspond to the ordered P4332 structure since the extra peaks at the wavenumbers mentioned above are observed. On the contrary, the absence of these peaks in samples ASP-2, ASP-3, ASP-4 and ASP-8 is representative of the disordered Fd-3m structure. Fig. 4(c) depicts the effect of calcination profile on crystallite size. Regarding the single-step calcination profiles, during the transition from 700°C to 800°C a clear increase in the crystallite size was observed (34.2 to 53.5 nm), while with further increase of calcination temperature a negligible increase in crystallite size was observed (~53.5 to 56.4 nm). A similar trend was also observed in the case of multi-stage calcination with a crystallite size range of 48.8-54.1 nm. Fig. 4(d) presents the calcination effect on the BET surface area of the materials. With increasing the calcination temperature, a decrease in the BET surface area was observed. In particular, a sharper decrease occurred mainly when the calcination temperature increased

from 700°C to 800°C (10.87 m2/g and 2.29 m2/g, respectively), while by further increase of temperature, the reduction of BET surface area was negligible.

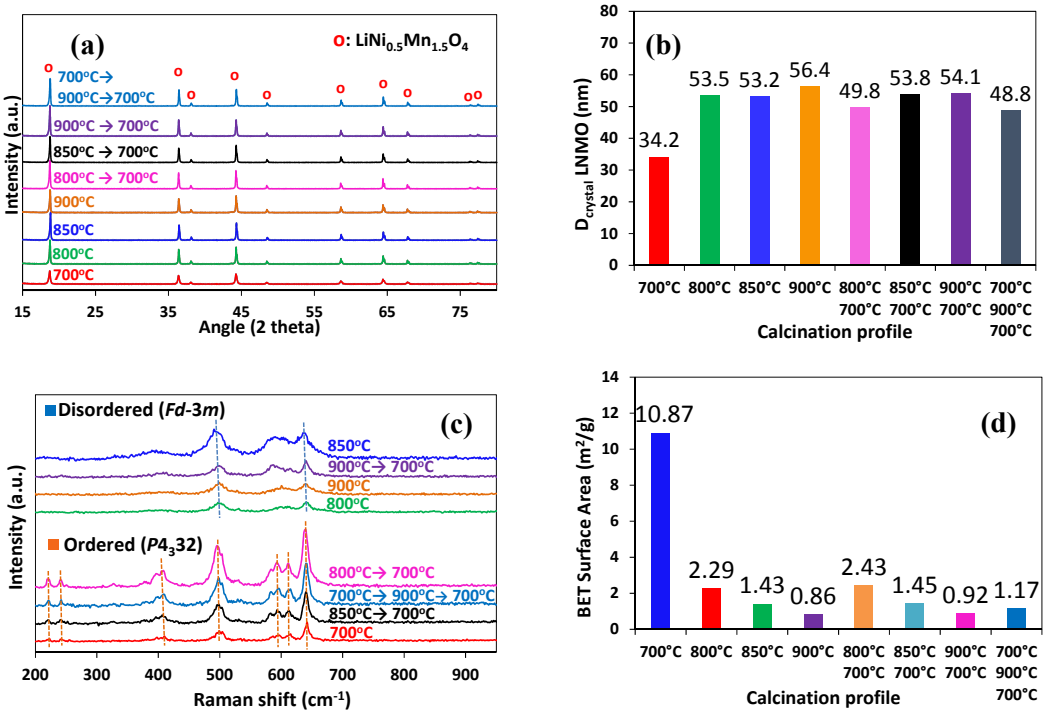

Fig. 4. (a) XRD spectra (b) crystallite size (c) Raman spectra and (d) BET surface area of ASP synthesised LNMO materials

According to SEM image in , all LNMO materials followed a spherical aggregate morphology consisting of smaller, dense particles. Concerning the morphology in the nano-scale, the materials consisted of non-spherical aggregates of primary particles ().

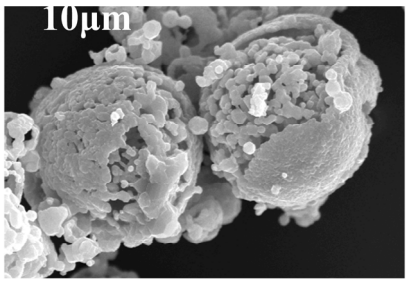

Fig. 5. Indicative SEM image of LNMO samples synthesised via ASP.

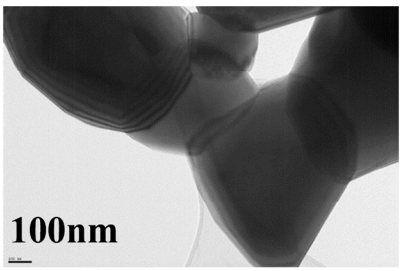

Fig. 6. Indicative TEM image of LNMO samples synthesised via ASP.

The electrochemical evaluation of LNMO materials was performed for C/10, C/5 and 1C charge/discharge rates. The results are presented in Fig. 7(a-h). With respect to one step calcination at 700°C (ASP-1), no activity was observed (Fig. 7(a)), while increasing the temperature at 800°C (ASP-2), a discharge specific capacity of ~ 110 mAh/g was obtained at C/10 followed by rapid value decrease over the five cycles, while the material had no specific capacity at 1C rate (Fig. 7(b)). By further increasing the calcination temperature to 850°C (ASP-3), the material exhibited a significant increase in discharge specific capacity at C/10 rate (~120 mAh/g) with very low

values at 1C rate (~10 mAh/g) (Fig. 7(c)). Similarly, at 900°C (ASP-4) the material exhibited a high discharge specific capacity at C/10 rate (~120 mAh/g), however with no activity at 1C (Fig. 7(d)).

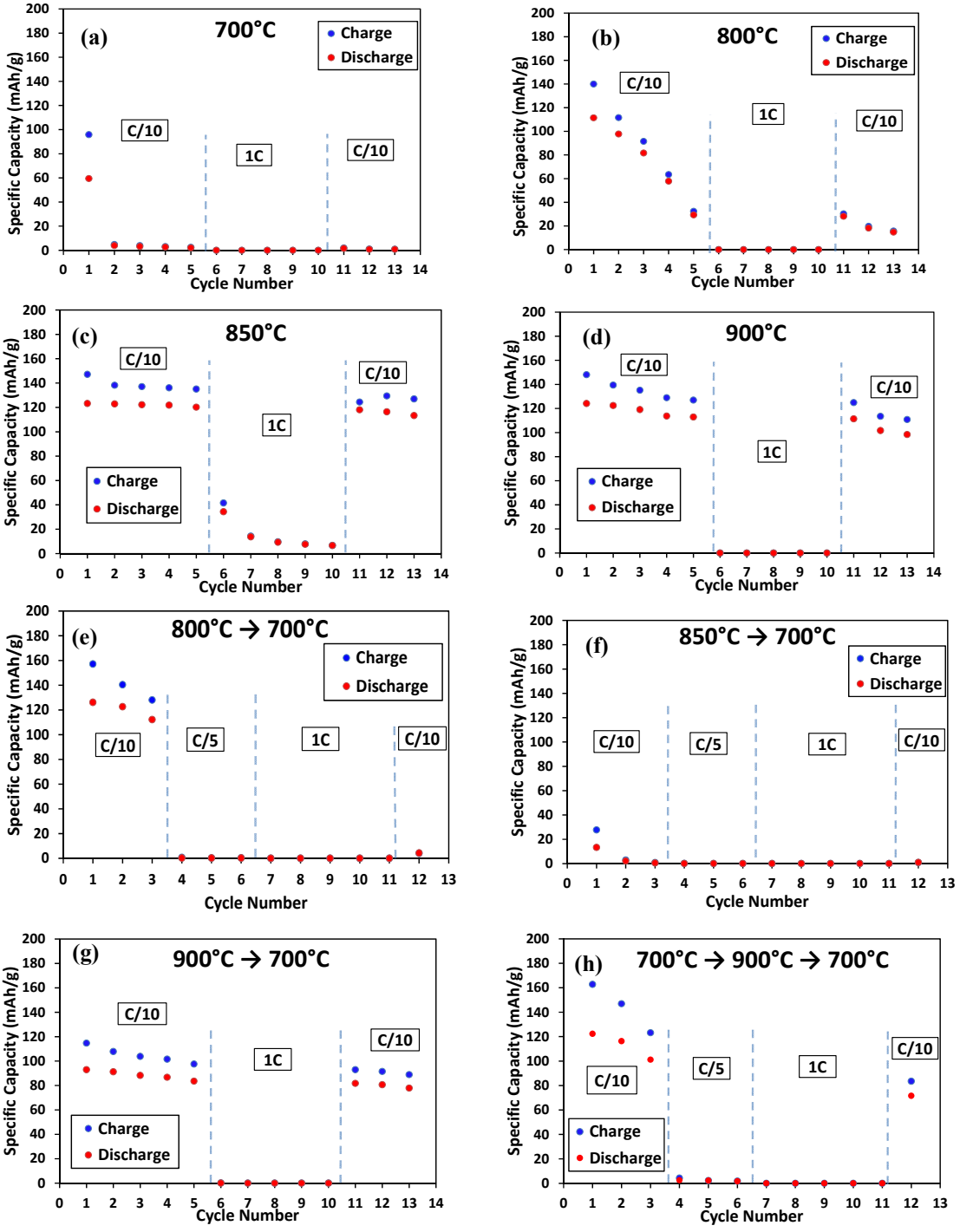

Fig. 7. Electrochemical performance of ASP synthesized LNMO calcined at (a) 700°C, (b) 800°C, (c) 850°C, (d) 900°C (e) 800°C → 700°C (f) 850°C → 700°C, (g) 900°C → 700°C, (h) 700°C → 900°C →700°C.

Concerning the multi-step calcination profiles, sample ASP-5 (800°C → 700°C) exhibited relatively high discharge specific capacity values (~120 mAh/g) at C/10 rate during the first cycles with rapid deactivation at the higher rates of C/5 and 1C (Fig. 7(e)), while sample ASP-6 (850°C → 700°C) shown no activity in the whole range of C-rates employed (Fig. 7(f)). Sample ASP-7 (900° C → 700° C) exhibited a relatively stable behaviour in the first five cycles at C/10 rate, demonstrating, however, lower specific capacity values and deactivation at 1C rate (Fig. 7(g)). Finally, sample ASP-8 (700°C → 900°C → 700°C) exhibited high initial capacity values, however with rapid reduction in the first three cycles (C/10) and deactivation at C/5 and 1C rates (Fig. 7(h)).

4. Conclusions

We have found that the synthesis of the cathode material $LiNi_{0.5}Mn_{1.5}O_4$ was possible with both LPSHS and ASP techniques. In the LPSHS method, increasing the metal ions/fuel molar ratio improved the electrochemical performance of LNMO. Despite the presence of impurities, the best performing material exhibited high stability over the cycles in all C-rates and good specific capacity values. Concerning the ASP method, calcination at temperatures ≥800°C led to the disordered *Fd-3m* space group of the spinel while the addition of a second calcination step (700°C) resulted in the ordered $P4_332$ space group. With respect to the electrochemical performance, the *Fd*-3*m* structure exhibited the optimum results, especially in the case of calcination at 850°C.

Based on the above results, it is evident that both LNMO synthesis technologies look promising for the realisation of active cathode materials based on the high-voltage spinel. It could be stated that ASP offers an advantage concerning the specific energy capacity. With ASP-synthesized materials, a specific energy capacity of higher than 80% of the theoretical one was obtained at C/10 rate. In the case of LPSHS, impurities led to somewhat less energy capacity. For the best performing ASP material a quite high irreversible capacity loss between the first charging and discharging cycle is noticed but after that, the difference between charging and discharging capacity seems to be stabilised. However, many more cycles are needed for a complete cyclability evaluation. The developed materials appear to perform very poorly at high C-rates (e.g. 1C). Nevertheless and based on the first results of further studies that are currently underway, this should be attributed to poor electrode electronic conductivity rather than the material itself. Electronic conductivity performance, is very much dependent on the cell formulation parameters, which, if not optimised on the basis of the main attributes of the material tested, can by itself result to to poor electrochemical performance. Such parameters are the carbon content used during the slurry formation as well as the electrode calendering level, thus the material density after the electrode coating process. These parameters have not been considered in the present study, so the resulting performance at high C-rates cannot lead to proper conclusions regarding the real potential of the ASP-synthesised cathodes. However, the C/10 performance is not fully retained after cycling at 1C and this could, to some extent, be attributed to structural degradation (e.g. Mn dissolution).

Further work should focus on reinforcing the lattice structural stability by the introduction of dopants and/or utilisation of protective coatings. Also, electrode formulation should be optimised and then tested for high C-rate performance and cyclability to fully investigate the potential of the developed LNMO materials.

Acknowledgements

We would like to thank the European Commission for funding this work through the HORIZON2020 eCAIMAN project (Grant No: GV-1-2014-653331).

References

[1] R. Ruffo, R.A. Huggins, C.M. Mari, M. Piana, W. Weppner, Ionics 11 (2005) 213–219.
[2] T.B. Reddy, D. Linden, Linden's Handbook of Batteries, fourth ed., McGraw-Hill, New York, 2011.
[3] M. Winter, J.O. Besenhard, M.E. Spahr, P. Novák, Adv. Mater. 10 (1998) 725–763.
[4] J.M. Tarascon, M. Armand, Nature 414 (2001) 359.
[5] J.B. Goodenough, Electrochemical cell with new fast ion conductors, US patent No. 4302518A, 1981, US.
[6] M. Wakihara, O. Yamamoto, Lithium ion batteries: fundamentals and performance, Wiley-VCH, New York, 1998.
[7] C. Miao, P.F. Bai, Q.Q. Jiang, X.Y. Wang, J. Power Sources 246 (2014) 232–238.
[8] D. Zhao, Y.L. Feng, Y.G. Wang, Y.Y. Xia, Electrochim. Acta 88 (2013) 632–638.

[9] S. Patoux, L. Daniel, C. Bourbon, C. Pagano, S. Jouanneau, S. Martinet, J. Power Sources 189 (2009) 344–352.
[10] D. Liu, W. Zhu, J. Trottier, F. Gagnon, C.M. Julien, J.B. Goodenough, K. Zaghib, RSC Adv. 4 (2014) 154–167.
[11] R. Santhanam, B. Rambabu, J. Power Sources 195 (2010) 5442–5451.
[12] S.H. Oh, K.Y. Chung, S.H. Jeon, C.S. Kim, W.I. Cho, B.W. Cho, J. Alloys Comp. 469 (2009) 244–250.
[13] M.G. Kim, J. Cho, Adv. Funct. Mater. 19 (2009) 1497–1514.
[14] J. Song, D.W. Shin, Y. Lu, C.D. Amos, A. Manthiram, J.B. Goodenough, Chem. Mater. 24 (2012) 3101–3109.
[15] M. Kunduraci, G.G. Amatucci, J. Electrochem. Soc. 153 (2006) A1345.
[16] K.M. Shaju, P. Bruce, Dalton Trans. 40 (2008) 5471–5475.
[17] K. Takahashi, M. Saitoh, M. Sano, M. Fujita, K. Kifune, J. Electrochem. Soc. 151 (2004) 173.
[18] T. Ohzuku, K. Ariyoshi, S. Yamamoto, J. Ceram. Soc. Jpn. 110 (2002) 501.
[19] D. Pasero, N. Reeves, V. Pralong, A. West, J. Electrochem. Soc. 155 (2008) A282–A291.
[20] Y. Idemoto, H. Narai, N. Kouta, J. Power Sources 119 (2003) 125–129.
[21] N. Amdouni, K. Zaghib, F. Gendron, A. Mauger, C.M. Julien, Ionics 12 (2006) 117.
[22] L. Wang, H. Li, X. Huang, E. Baudrin, Solid State Ionics 193 (2011) 32–38.
[23] N.P.W. Pieczonka, Z. Liu, P. Lu, K.L. Olson, J. Moote, J.-H. Kim, J. Phys. Chem. C 117 (2013) 15947–15957.
[24] L. Wang, D. Chen, J. Wang, G. Liu, W. Wu, G. Liang, Powder Technology 292 (2016) 203–209.
[25] H. Fang, L. Li, G. Li, J. Power Sources 167 (2007) 223–227.
[26] J. Zheng, J. Xiao, X. Yu, L. Kovarik, M. Gu, F. Omenya, X. Chen, X.Q. Yang, J. Liu, G.L. Graff, M.S. Whittingham, J.G. Zhang, Phys. Chem.
Chem. Phys. 14 (2012) 13515–13521.
[27] Z. Zhu, H. Yan, D. Zhang, W. Li, Q. Lu, J. Power Sources 224 (2013) 13–19.
[28] Y.J. Gu, Y. Li, Y. Fu, Q.F. Zang, H.Q. Liu, J.X. Ding, Y.M. Wang, H.F. Wang, J. Ni, Electrochim. Acta 176 (2015) 1029–1035.
[29] J. Feng, Z. Huang, C. Guo, N.A. Chernova, S. Upreti, M.S. Whittingham, Appl. Mater. Interfaces 5 (2013) 10227–10232.
[30] H.B. Lin, Y.M. Zhang, H.B. Rong, S.W. Mai, J.N. Hu, Y.H. Liao, L.D. Xing, M.Q. Xu, X.P. Li, W.S. Li, J. Mater. Chem A 2 (2014) 11987–11995.
[31] G. Liu, X. Kong, H. Sun, B. Wang, Ceram. Int. 40 (2014) 14391–14395.
[32] L. Wen, Q. Lu, G. Xu, Electrochim. Acta 51 (2006) 4388–4392.
[33] J.H. Kim, S.T. Myung, Y.K. Sun, Electrochim. Acta 49 (2004) 219–227.
[34] S.T. Myung, S. Komada, N. Kumagai, H. Yashiro, H.T. Chung, T.H. Cho, Electrochim. Acta 47 (2002) 2543–2549.
[35] Y.S. Lee, Y.K. Sun, S. Ota, T. Miyashita, M. Yoshio, Electrochim. Commun. 4 (2002) 989–994.
[36] Y. Xue, Z. Wang, F. Yu, Y. Zhang, G. Yin, J. Mater. Chem. A 2 (2014) 4185–4191.
[37] A. Kraytsberg, Y. Ein-Eli, Adv. Energy Mater. 2 (2012) 922–939.
[38] T.-F. Yi et al., Journal of Power Sources 316 (2016) 85–105.
[39] H. Wang, J. Nanosci. Nanotechnol. 15 (2015) 6883–6890.
[40] A.V. Potapenko et al., Journal of Energy Chemistry 23 (2014) 543–558.
[41] S.-T. Myung et al., Journal of Power Sources 283 (2015) 219–236.
[42] X.L. Xu, S.X. Deng, H. Wang, J.B. Liu, H. Yan, Nano-Micro Lett. 9: 22 (2017).
[43] M.P. Pechini, Method of preparing lead and alkaline earth titanates and niobates and coating method using the same to form a capacitor, US Patent No. 3330697, US.
[44] S. Lorentzou, C. Pagkoura, A. Zygogianni, G. Kastrinaki, A.G. Konstandopoulos, SAE Int. J. Mater. Manf. 1 (2009) 189–198.
[45] K.G. Sakellariou, G. Karagiannakis, Y.A. Criado, A.G. Konstandopoulos, Solar Energy 122 (2015) 215–230.
[46] J. Obermeier, K.G. Sakellariou, N.I. Tsongidis, D. Baciu, G. Charalambopoulou, T. Steriotis, K. Müller, G. Karagiannakis, A.G. Konstandopoulos, A. Stubos, W. Arlt, Solar Energy 150 (2017) 298–309.
[47] K. Karadimitra, E. Papaioannou, A.G. Konstandopoulos, PARTEC (2001) 97.
[48] S. Lorentzou, C.C. Agrafiotis, A.G. Konstandopoulos, Granular Matter 10 (2008) 113–122.
[49] S. Lorentzou, A. Zygogianni, K. Tousimi, C. Agrafiotis, A.G. Konstandopoulos, Journal of Alloys and Compounds 483 (2009) 302–305.
[50] S. Lorentzou, G. Kastrinaki, C. Pagkoura, A.G. Konstandopoulos, Nanoscience and Nanotechnology Letters 3 (2011) 697–704.